
COMBINING DATA ASSIMILATION AND MACHINE LEARNING TO ESTIMATE PARAMETERS OF A CONVECTIVE-SCALE MODEL

A PREPRINT

S. Legler

Meteorological Institute
Ludwig-Maximilians-Universität
Munich, Germany
S.Legler@physik.uni-muenchen.de

T. Janjić

Meteorological Institute
Ludwig-Maximilians-Universität
Munich, Germany

September 8, 2021

ABSTRACT

Errors in the representation of clouds in convection permitting numerical weather prediction models can be introduced by different sources. These can be the forcing and boundary conditions, the representation of orography, the accuracy of the numerical schemes determining the evolution of humidity and temperature, but large contributions are due to the parametrization of microphysics and the parametrization of processes in the surface and boundary layers. These schemes typically contain several tunable parameters that are either not physical or only crudely known, leading to model errors. Traditionally, the numerical values of these model parameters are chosen by manual model tuning. More objectively, they can be estimated from observations by the augmented state approach during the data assimilation.

Alternatively, in this work, we look at the problem of parameter estimation through an artificial intelligence lens by training two types of artificial neural networks (ANNs) to estimate several parameters of the one-dimensional modified shallow-water model as a function of the observations or analysis of the atmospheric state. Through perfect model experiments we show that Bayesian neural networks (BNNs) and Bayesian approximations of point estimate neural networks (NNs) are able to estimate model parameters and their relevant statistics. The estimation of parameters combined with data assimilation for the state decreases the initial state errors even when assimilating sparse and noisy observations. The sensitivity to the number of ensemble members, observation coverage and neural network size is shown. Additionally, we use the method of layer-wise relevance propagation to gain insight into how the ANNs are learning and discover that they naturally select only a few grid points that are subject to strong winds and rain to make their predictions of chosen parameters.

Keywords convective scale data assimilation · parameter estimation · Bayesian neural network · EnKF · layer-wise relevance propagation

1 Introduction

In recent years machine learning (ML) has become a subject of interest in various research fields within atmospheric physics. Attempts of including ML into climate and weather modeling reach from using it to represent sub-grid processes in global climate models [O’Gorman and Dwyer, 2018, Rasp et al., 2018, Yuval and O’Gorman, 2020], over replacing data assimilation (DA) by an artificial neural network (ANN) to emulate the ensemble Kalman filter [EnKF, Cintra and de Campos Velho, 2014], to utilizing an ANN as a surrogate for the complete physical model [Brajard et al., 2020] or for the model error [Farchi et al., 2021] during the DA. Bonavita and Laloyaux [2020] use ANNs to estimate model error tendencies in the Integrated Forecasting System (IFS) of the European Centre for Medium-Range Weather Forecasts (ECMWF) and show that they are able to emulate the main outcomes acquired by the weak-constraint four dimensional variational (4D-Var) algorithm. Furthermore, computational cost can be improved when including ML in the DA. For example, Ruckstuhl et al. [2021] used a convolutional neural network (CNN) to show that a hybrid of a

CNN and the EnKF is able to decrease the analysis/background error, equivalent to results obtained by the quadratic programming ensembles [Janjić et al., 2014, QPEns] but with a reduced computational cost compared to that of the QPEns. Finally, ML approaches can also be improved with DA methods by replacing the backpropagation during the training with an adaptive EnKF [Trautner et al., 2020].

While there are many examples of using ML to enhance the analysis/forecast of the model state, deep learning for model parameter estimation is not well developed, especially on the convective scale. In Yadav et al. [2020] the coupling parameter of the two-level Lorenz-96 model [Lorenz, 2005] is estimated as a function of the resolved, large-scale state variable using a Gaussian Process (GP) [Rasmussen and Williams, 2006]. The GP was compared to two types of ANNs and a simple linear regression and outperformed the other methods in most of the experiments. Similarly, data assimilation has been successfully used in geosciences for estimation of the state from sparse and noise observations. However, when parameters are jointly estimated with the state several problems arise, for example, parameters are not directly observed and therefore updated through cross-correlations which might not be accurate; parameter values often need to be within certain bounds therefore Gaussian assumptions of data assimilation algorithms are not valid and finally to use data assimilation for parameter estimation, stochastic model for the parameters needs to be pre-specified to keep the spread in parameters [Ruckstuhl and Janjić, 2018, 2020]. In this study, we investigate a possibility of using data assimilation for the state estimation while using ML for parameter estimation in order to overcome some of the problems of augmented state approach for estimating parameters from observations via data assimilation.

Although ML algorithms show promising results in idealized test cases, they come with two major drawbacks. On one hand, ANNs typically do not provide an uncertainty with their predictions, which makes it hard to ascribe a confidence when using them in operational settings. On the other hand, they are still seen as black boxes that do not provide any insight into the functions they are trying to approximate. To tackle the latter problem Toms et al. [2020] introduced layer-wise relevance propagation (LRP) to the geosciences, which can be used to visualize how the ANN makes its prediction. Labe and Barnes [2021] utilized this method to disentangle relative influences on regional surface temperatures of aerosols and greenhouse gases in the atmosphere. The former drawback could be approached by using stochastic ANNs instead of their widely used deterministic counterpart. The goal of this study is threefold. First, to estimate parameters of the convective-scale modified shallow water model from sparse and noisy observations using ML and DA. Second, to compare the predictions and statistics of stochastically trained Bayesian neural networks (BNNs) with ensemble of deterministically trained point estimate neural networks. And third, to visualize the decision making of the ANNs by applying LRP.

The paper is organized as follows. The model and the DA for the state are described in Section 2. Section 3 introduces two ML algorithms for parameter estimation, and their use in combination with DA. This is followed by an investigation of the performance of these two hybrid algorithms in state and parameter space in Section 4. A final discussion and some perspectives are presented in Section 5.

2 Dynamical model and state estimation

2.1 Modified shallow water model

For this study the same dynamical model, model parameters, and parameter bounds (Table 1) as in Ruckstuhl and Janjić [2018] were used to conduct the experiments. However, instead of using data assimilation with augmented state approach for parameter estimation, we estimate the parameters with ANNs. In the *twin experiments* presented in this study the true state (*nature run*) of the atmosphere is generated by the modified shallow water model [Würsch and Craig, 2014]. Synthetic observations are produced by adding random perturbations to the true state. This model is computationally inexpensive but still represents the key space and time scales of storm developments. It is based on the shallow water equations for the fluid velocity u and the fluid height h with a modification of the geopotential ϕ to include conditional instability. Additionally, a variable for the rain r was added to mimic nature. The equations are as follows:

$$\frac{\partial u}{\partial t} + u \frac{\partial u}{\partial x} + \frac{\partial(\phi + c^2 r)}{\partial x} = \beta_u + D_u \frac{\partial^2 u}{\partial x^2} \quad (1)$$

$$\phi = \begin{cases} \phi_c & \text{if } h > h_c \\ gh & \text{else} \end{cases} \quad (2)$$

$$\frac{\partial r}{\partial t} + u \frac{\partial r}{\partial x} = D_r \frac{\partial^2 r}{\partial x^2} - \alpha r - \begin{cases} \delta \frac{\partial u}{\partial x} & \text{if } h > h_r \text{ and } \frac{\partial u}{\partial x} < 0 \\ 0 & \text{else} \end{cases} \quad (3)$$

$$\frac{\partial h}{\partial t} + \frac{\partial(uh)}{\partial x} = D_h \frac{\partial^2 h}{\partial x^2} \quad (4)$$

- D_u, D_r, D_h : diffusion constants
- $c^2 = g \times h_0$: gravity-wavespeed for absolute fluid layer $h_0 (h_0 < h_c)$
- δ : production rate of rain
- α : removal rate of rain

Convection is triggered by adding a low amplitude noise source β_u at random locations to the velocity at every model time step. When the fluid height h exceeds the threshold h_c , which represents the level of free convection, the geopotential is replaced by a lower constant value ϕ_c . The gradient of the geopotential forces fluid to the regions of lower geopotential, which then builds up the fluid height in those regions. Once h reaches the threshold h_r rain is being produced by adding rainwater mass to the geopotential. The removal of rain is mimicked by a linear relaxation towards zero. For the experimental set-up a one dimensional grid of length 125 km with 250 grid points was used, which yields a state vector of the form:

$$\mathbf{x} = \begin{bmatrix} \mathbf{u} \\ \mathbf{h} \\ \mathbf{r} \end{bmatrix} \in \mathbb{R}^{750}. \quad (5)$$

The model parameters which were chosen to be estimated are the rain removal rate α , the low constant value for the geopotential ϕ_c and the threshold for the fluid height h_r while the other parameters were known during the experiments. Assuming all of the model parameters are constant in space the resulting parameter vector is:

$$\theta = \begin{bmatrix} \alpha \\ \phi_c \\ h_r \end{bmatrix} \in \mathbb{R}^3. \quad (6)$$

Observations are generated from the nature run every 60 model time steps by adding a Gaussian error to u and h and a lognormal error to r variable to keep its positivity. To simulate radar data only the grid points where $r > 0.005$ were observed. Furthermore, wind observations of 25% of the remaining grid points were added. The model parameters for the nature run are taken from uniform distributions. The upper and lower bounds of the uniform distributions for the model parameters as well as biases and standard deviations of the observational errors are summarized in Table 1 and Table 2 respectively.

Parameter	Lower Bound	Upper Bound
α	0.0003	0.001
ϕ_c	899.7	899.9
h_r	90.15	90.25

Table 1: Lower and upper bounds for the uniform distributions of the model parameters

Variable	Mean	Standard Deviation
u	0	0.001
h	0	0.02
r	0.001	1e-7

Table 2: Means and standard deviations for the distributions of the observational errors

2.2 Stochastic ensemble Kalman filter

Since the focus of this work is testing new algorithms for parameter estimation, a simple stochastic EnKF [Evensen, 1994, 2003] will be utilized for all experiments. It is based on the following cost function for each of the N_{ens} ensemble members:

$$J(\mathbf{x}_t^{a,i}) = (\mathbf{x}_t^{f,i} - \mathbf{x}_t^{a,i})^T \mathbf{P}_t^{-1} (\mathbf{x}_t^{f,i} - \mathbf{x}_t^{a,i}) + (\mathbf{y}_t^i - \mathbf{H}_t \mathbf{x}_t^{a,i})^T \mathbf{R}_t^{-1} (\mathbf{y}_t^i - \mathbf{H}_t \mathbf{x}_t^{a,i}) \quad (7)$$

where $i, i = 1 \dots N_{ens}$ denotes one ensemble member, $\mathbf{x}_t^{f/a,i}$ are the background and analysis states respectively, \mathbf{R}_t is the observation-error covariance matrix and \mathbf{H}_t denotes the observation operator, that maps the model states to the observation space. In this work we assume \mathbf{H}_t to be linear. $\{\mathbf{y}_t^i\}$ represents an ensemble of observations acquired by perturbing the observation vector \mathbf{y}_t such that $\mathbf{y}_t^i = \mathbf{y}_t + \epsilon^i$. ϵ^i is a perturbation taken from a distribution with a bias and a standard deviation that represent the observation error. The subscript t refers to the time when a DA cycle is being carried out, which usually corresponds to the time appropriate observations are available. For the rest of this chapter, the subscript t will be withheld. The forecast-error covariance matrix is generated with the ensemble of background states:

$$\mathbf{P} = \overline{(\mathbf{x}^{f,i} - \bar{\mathbf{x}}^f)(\mathbf{x}^{f,i} - \bar{\mathbf{x}}^f)^T} \quad (8)$$

Architecture		
Type of Layer	Size (input x output)	Activation Function
Linear	750 x 31	ReLU
Batch-Norm	31 x 31	None
Dropout (p=0.5)	31 x 31	None
Linear	31 x 19	ReLU
Linear	19 x 11	ReLU
Linear	11 x 3	None
Training		
Optimizer	Adam	
Mini-Batch-Size	32	
Number of Epochs	150	

Table 3: Architecture and training specifics of the NN

where the overline denotes the average over the ensemble members. Minimizing J for each ensemble member yields the analysis ensemble:

$$\mathbf{x}^{a,i} = \mathbf{x}^{f,i} + \mathbf{P}\mathbf{H}^T(\mathbf{H}\mathbf{P}\mathbf{H}^T + \mathbf{R})^{-1}(\mathbf{y}^i - \mathbf{H}\mathbf{x}^{f,i}) \quad (9)$$

with the Kalman gain $\mathbf{K} = \mathbf{P}\mathbf{H}^T(\mathbf{H}\mathbf{P}\mathbf{H}^T + \mathbf{R})^{-1}$. In all experiments exhibited in this study Equation (9) was used to estimate only the atmospheric state. Once analysis ensemble and corresponding parameters (see Section 3) are estimated, nonlinear model (1) - (4) would be used to obtain forecast ensemble $\mathbf{x}^{f,i}$ for time $t + 1$.

3 ML for parameter estimation

The scientific objective of this study is to estimate three model parameters of the modified shallow water model as a function of the atmospheric state consisting of the atmospheric variables u, h, r using different types of ANNs.

3.1 Types and architecture of ANNs

Two types of ANNs are utilized - a *deep ensemble of point estimate neural networks (NN)* and a *Bayesian neural network (BNN)*. Both have an input size of 750 - three atmospheric variables for each of the 250 grid points - and an output size of three which corresponds to the three global, unknown parameters that are wished to be estimated. The term point estimate neural network is used in this work to refer to the standard type of neural network which given an input predicts one deterministic output. To quantify the uncertainty of the estimation produced by the NN the method of deep ensembles from Lakshminarayanan et al. [2017] is adopted. This is an easy implementable approach, where an ensemble of neural networks $\{NN_k\}_{k=1}^{n_{NN}}$ consisting of n_{NN} members with the same architecture but random initial weights is trained independently. The definition of BNNs is not completely consistent across literature. We adopt its definition from Jospin et al. [2020] as a type of ANN "...built by introducing stochastic components into the network..." and trained using *Bayesian inference* [MacKay, 1992]. Stochastic components can either be introduced as probability distributions over the activation functions or over the weights, although for this study the latter one is utilized as this is the more common one. For a more detailed account about the differences between NNs and BNNs and how to utilize BNNs we refer to Jospin et al. [2020]. For both ANNs (Tables 3 and 4) fully connected linear layers were chosen with additional batch normalization layers to accelerate the training [Ioffe and Szegedy, 2015]. For the NN a dropout layer was added to reduce overfitting [Labach et al., 2019] which was not necessary for the BNN. *ReLU* was used as the activation function for all hidden layers of the NN. This was not possible for the BNN as it resulted in the *dying ReLU problem* [Lu, 2020] which is a widely known phenomenon where ReLU neurons output 0 for all inputs. To combat this the *LeakyReLU* was utilized for all hidden layers of the BNN. The activation functions are defined as:

$$ReLU(x) = \max(0, x) \quad (10)$$

$$LeakyReLU(x) = \max(0, x) + 0.01 * \min(0, x). \quad (11)$$

The number of neurons for the hidden layers were optimized independently for the NN and the BNN and therefore differ from each other.

3.2 Data generation and training

To generate the input-output pairs for the training, validation, and test data-sets 100 000 sets of parameters are taken randomly from the uniform distributions specified in Table 1. For each set of parameters Equations (1) to (4) are solved for 1000 model time steps with a timestep discretization of $\Delta t = 4$. Snapshots in time at $t = 1000$ of the state vectors are used as the input of the ANNs. The parameters used to generate those states are the corresponding outputs after

Architecture			Stochastic Model	
Type of Layer	Size (input x output)	Activation Function	Priors $p(W_i^{(k,l)})$	$\mathcal{N}(0, 1)$
Batch-Norm	750 x 750	None	Variational distributions $q_\phi(W_i^{(k,l)})$	$\mathcal{N}(\mu, \sigma)$
Linear	750 x 20	LeakyReLU	Training	
Linear	20 x 20	LeakyReLU	Optimizer	Adam
Linear	20 x 20	LeakyReLU	Mini-Batch Size	32
Linear	20 x 3	None	Number of Epochs	3

Table 4: Architecture, stochastic model and training specifics of the *BNN*

rescaling them to $[0,1]$. From these 100 000 input-output pairs 90% are used for training, 5% for validation during the training and 5% for testing. Additionally, the input samples are augmented during the training by adding perturbations taken from distributions with means and standard deviations corresponding to the observational error specified in Table 2. For each input sample three perturbed samples are added during the training resulting in a training size of 360000. The NN is trained via stochastic gradient descent. Since computing the exact Bayesian posterior of the BNN is usually intractable, we utilize the optimization method of stochastic variational inference [Hoffman et al., 2013] where a set of variational distributions is approximated to the exact Bayesian posteriors during the training. A widely used default for the prior weights of BNNs are normal distributions with mean 0 and standard deviation σ [Jospin et al., 2020]. After evaluating the trained weights of the point estimate neural networks it seemed appropriate to set $\sigma = 1$. To simplify training, the variational distributions are initialized as normal distributions as well such that during the training only the means and standard deviations have to be optimized. For both ANNs an adaptable learning rate [Kingma and Ba, 2014, Adam] was chosen with an initial value of 0.001. The NN is implemented and trained using only the library PyTorch [Paszke et al., 2019] while for the BNN also the probabilistic programming language Pyro [Bingham et al., 2018] which is built on top of PyTorch is used.

3.3 Combining DA and ML

All DA experiments presented in this study are conducted as twin experiments. The atmospheric state and model parameters of the nature run start from a sample taken from the test data-set. The state is propagated forward in time using the modified shallow water model while the parameters are kept constant. The background ensemble members start from different states. Whenever a DA cycle is performed according to Equation (9) the model parameters are estimated according to one of the following set-ups.

1. **true**: The true values of the parameters are known and used for the background state throughout all DA cycles.
2. **random**: The true values of the parameters are not known and picked randomly from a the uniform distributions specified in Table 1.
3. **NN**: The parameters are estimated using the observations (DA cycle = 0) or the analysis (DA cycle > 0) as input to an ensemble of NNs with 15 members trained according to Section 3.2.
4. **BNN₀**: The parameters are estimated using the observations (DA cycle = 0) or the analysis (DA cycle > 0) as input to a BNN (BNN₀) trained according to Section 3.2.
5. **BNN₀+BNN_t**: The parameters are estimated using the observations as input to BNN₀ (DA cycle = 0) or to BNN_t (DA cycle > 0) trained according to Section 3.3.1.

The parameter estimates are then used as parameters for the forward model simulations with the modified shallow water model for the next 60 model time steps until the next DA cycle is performed, and parameters are estimated again with ML algorithm.

3.3.1 Remarks

DA cycle = 0: For the first DA cycle, the observations taken from the nature run are used as inputs for the ANNs. If a variable is only partially observed the unobserved grid points are interpolated with a quadratic interpolation for u and h . For r the unobserved grid points are simply set to 0.

NN: At DA cycle > 0 each analysis ensemble member $\mathbf{x}_t^{a,i}$ is used as input for each NN ensemble member resulting in $15 \cdot N_{ens}$ parameter estimates. To obtain N_{ens} parameter vectors out of this ensemble a beta distribution is fitted to the ensemble of parameter estimates. The parameters for each state ensemble member is then taken from this beta distribution.

BNN_t: This set-up is chosen to test the feasibility of online training during the DA cycle with a realistic number of forecast/analysis ensemble members. Since the training size of BNN_t is much smaller than that used for BNN₀ it is necessary to reduce the number of trainable weights for BNN_t. The first modification is to reduce the input size.

Experiments from Ruckstuhl and Janjić [2018] indicate that the rain r and fluid height h are stronger correlated to the parameters than the wind u . Hence, instead of using all 3 atmospheric variables as the input, only r and h are used. Since BNN_t is trained from scratch at each DA cycle, the input size can be left variable. This allows to only train on those grid points that are actually observed. Additionally, because we assume the true parameters to be constant over the whole grid, it might not be necessary to use all observed grid points as input. Therefore if more than 62 gridpoints (about 25 % of the whole grid) are observed, only those 62 grid points with the highest observed values for r are used. $\tilde{\mathbf{x}}_\tau^{f,i}$ in Equation (12) refers to this reduced background state. To further reduce the number of learnable weights, the number of neurons per hidden layer is decreased from 20 to 2. In total, this results in a maximum of around 540 learnable weights. The resulting input for the training is then given by

$$\mathbf{H}_t \tilde{\mathbf{x}}_\tau^{f,i} + \epsilon^i \quad (12)$$

with the observation operator \mathbf{H}_t and $i = 1, \dots, N_{ens}$. The 10 previous points in time $\tau = t-9, \dots, t$ are used to increase the training size from N_{ens} to $N_{ens} \cdot 10$. The labels for these inputs are simply the model parameters θ_{t-60}^i from the previous estimation. Noise corresponding to the observational error specified in Table 2 was added during the training for the same reasons as for the training from Section 3.2. The stochastic model, optimizer, and mini-batch size are the same as for BNN_0 but 9 training epochs were necessary to reach a minimum in the validation loss which is most likely caused by the reduced training size.

4 Results

4.1 Diagnostics

Besides the standard diagnostic tools - Root Mean Squared Error (RMSE), ensemble spread (spread), and Coefficient of Determination (R^2) - we utilize *LRP* in this study. *LRP* is a visualization tool, which takes a trained ANN and an ANN input sample as the input and produces a *LRP heatmap* as the output. The *LRP heatmap* is a vector of the same size as the ANN input and those entries with higher numerical values can be interpreted as being more relevant for the ANN’s prediction as the ones with lower values. This method has been introduced first to the field of computer vision by Bach et al. [2015] and the *PyTorch* implementation used in this study is from Böhle et al. [2019]. For an in-depth explanation of the algorithm, we refer to Toms et al. [2020], who recently introduced *LRP* to the geosciences. The underlying idea of *LRP* is to calculate a *relevance* for each input pixel by taking a specific ANN output, which in this case would be either α , ϕ_c or h_r , and propagating it back through the network according to a certain set of propagation rules. Applying *LRP* to the ANNs trained in this study could thus give insight into which grid points and atmospheric variables are most relevant for each of the three parameters.

4.2 Evaluation

For the first performance evaluation 500 samples from the test dataset were used to estimate the parameters. For these experiments we assume a fully observed grid and no observation noise. Each output ensemble was averaged and then plotted against its corresponding ground truth (Figure 1). Additionally, as a baseline model a simple linear regression (LR) model was fitted to the same training data. As a benchmark, the ideal output was plotted as well, which corresponds to the black lines with slope 1. The BNN outperforms the NN as well as the LR in all three parameters while the LR has the lowest R^2 scores for all parameters (Table 5). While the BNN has similar R^2 scores for the different parameters the NN’s and LR’s performance varies greatly between them. For h_r the LR performs even worse than a baseline model which would predict the average value of the parameter bounds for all inputs. The scatter plot in Figure 1 emphasizes that both ANNs are slightly overestimating low parameter values while underestimating high ones while the LR predicts values that are greatly out of bounds for all parameters.

model	α	ϕ_c	h_r
NN	0.53	0.44	0.62
BNN	0.79	0.74	0.75
LR	0.41	0.26	-0.52

Table 5: R^2 of the parameter predictions plotted in Figure 1 for NN, BNN and LR

model	α	ϕ_c	h_r
NN	16%	18%	14%
BNN	9%	11%	10%
LR	17%	19%	26%

Table 6: Averaged error relative to the width of the bounds from Table 1 in % of the parameter predictions plotted in Figure 1 for NN, BNN and LR

The remaining experiments presented in this subsection are conducted according to Section 3.3 and if not stated otherwise averaged over 100 individual experiments with different ground truth values. Since NN and BNN_0 are

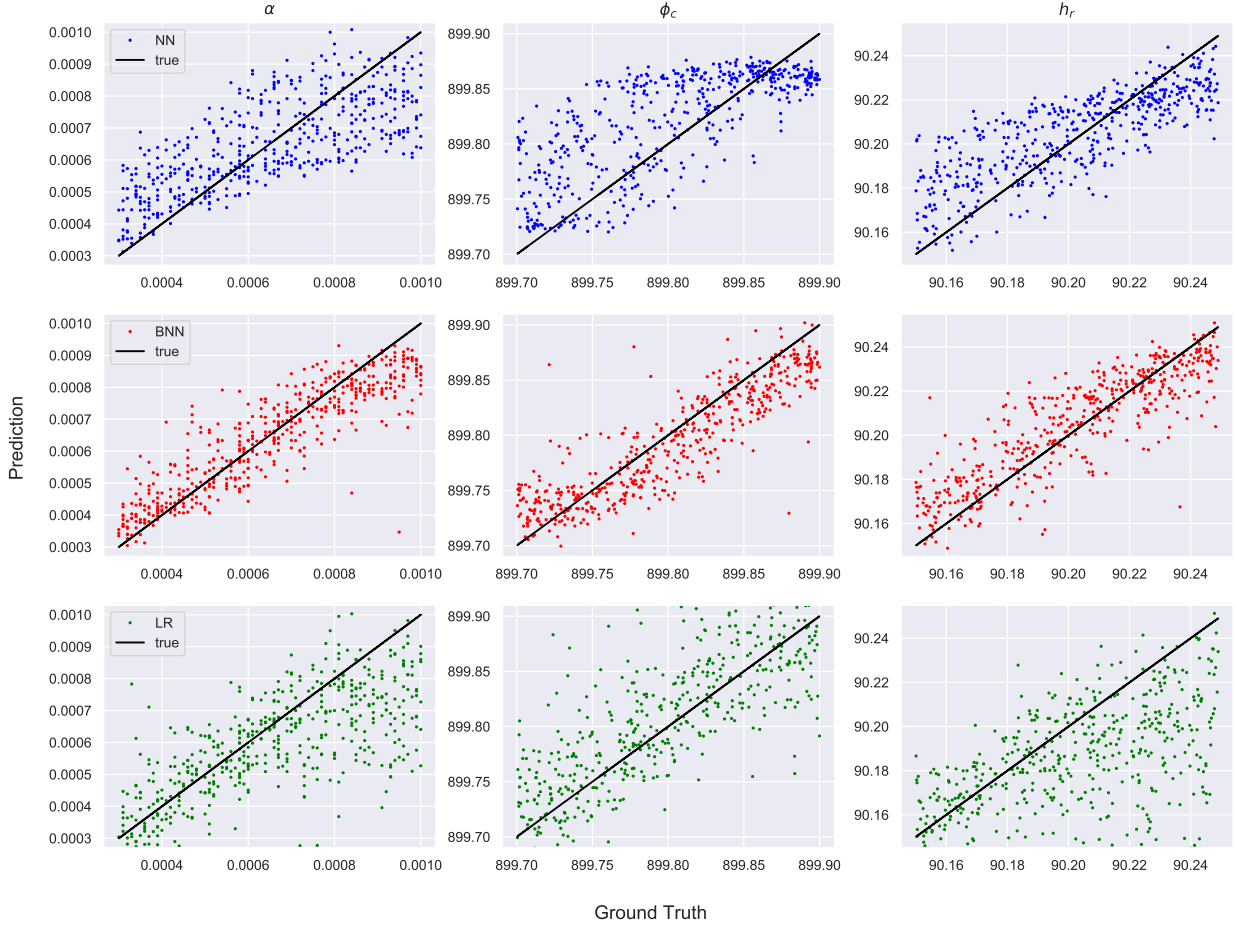


Figure 1: Output of NN (blue dots), BNN (red dots), and LR (green dots) against corresponding ground truths and ideal output (black lines) of 500 samples

trained on snapshots of model states from one point in time, the question arises how they perform when using states from later points in time as the input and comparing them with BNN_t which is constantly retrained over time. If the predictive power of the former do not significantly decrease it would only be necessary to train the ANNs once and they could then be used to predict parameters whenever necessary which would be computationally cheap. In Figure 2 the parameter RMSEs and parameter ensemble spreads of all ANNs are plotted against time in DA cycles where DA cycle = 0 corresponds to the time NN and BNN_0 were trained on and between two points on the x-axis lie 60 model time steps. The RMSE of the parameters is smallest at the beginning of the time evolution. After that, they grow for about 50 cycles and then oscillate around a relatively constant value (Figure 2, left). Although BNN_0 outperforms the NN for the initial estimate at DA cycle = 0 over time the RMSEs increase a lot faster for BNN_0 compared to NN. For $BNN_0 + BNN_t$ the RMSEs also increase over time, but to a lesser extent compared to the other methods. While the parameter spread of the BNNs increases which is in accordance to the increased RMSEs the spread of the NN actually decreases over time (Figure 2, right) which could be interpreted as the NN becoming more confident in its prediction over time.

Histograms of the parameter estimation of h_r for one single experiment were plotted for the NN as well as for both BNN methods (Figure 3). Since this is only a single experiment the results shown here are not statistically significant. However, they still illustrate the key differences between the methods. To also investigate the change of the distributions over time a histogram for each method was plotted from $t=0$ (DA cycle = 0) to $t=240$ (DA cycle = 4). While the NN estimates are spread out over the whole range with accumulations around the true value the estimates of the BNNs are close to Gaussian distributions with the mean near the true value and a small variance. Nonetheless, over time the prediction of BNN_0 spreads out and it loses its predictive power for $DA_{cycle} \geq 4$. Since BNN_0 starts predicting parameters that lie greatly outside of the bounds it was necessary to map the outliers to the bounds as otherwise

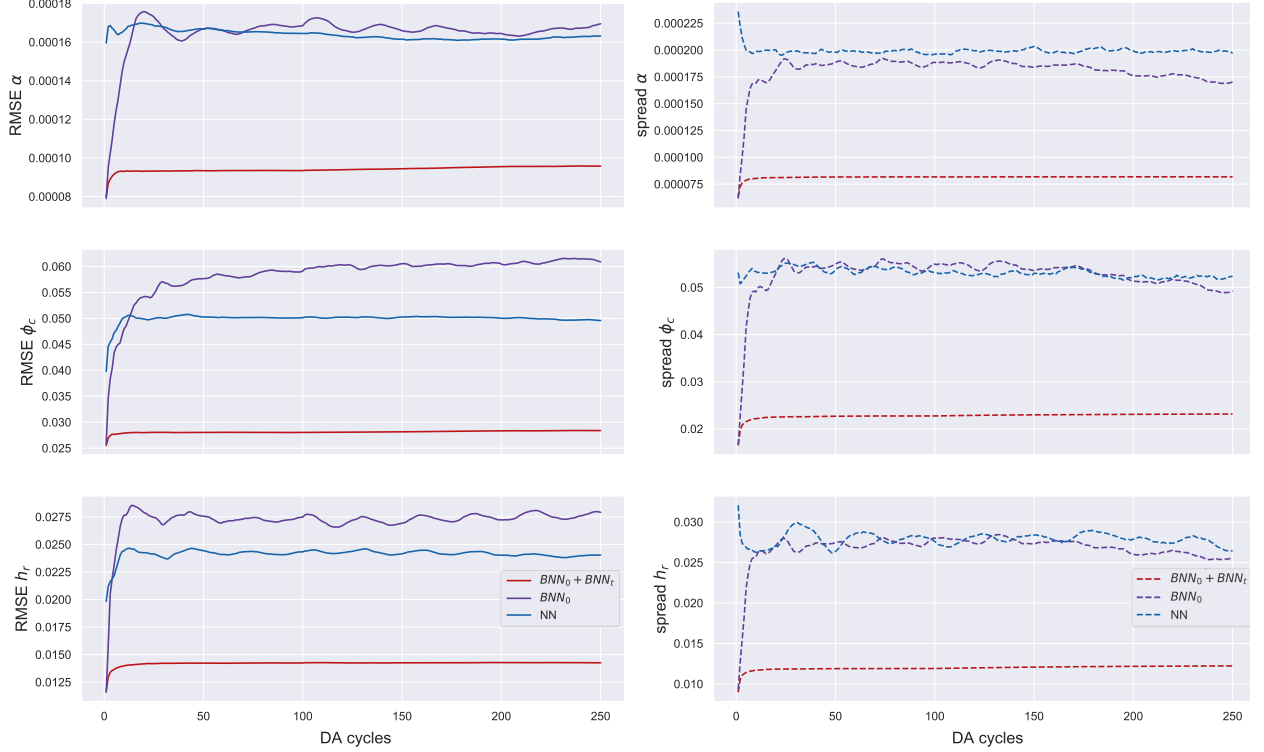


Figure 2: Time evolution of RMSE (left) and ensemble spread (right) of parameter estimates against time in DA cycles with 50 analysis ensemble members averaged over 100 experiments

the modified shallow water model could not run which explains the aggregations near the edges. Since this was not necessary for the other two methods the remaining experiments were only conducted using NN and $BNN_0 + BNN_t$.

The sensitivity of the RMSE and ensemble spread of the atmospheric variable and the model parameter estimates to the number of state ensemble members (Figure 4) and observation coverage (Figure 6) is studied for NN and $BNN_0 + BNN_t$ to compare their performance and statistics with the best (black) and worst (gray) case scenarios and to investigate the capabilities of the ANNs under sparse and noisy conditions. For all methods 100 experiments with 250 DA cycles each are conducted and averaged over the last 100 DA cycles. As expected, the RMSEs of the atmospheric variables decrease for all setups with an increase in state ensemble members (Figure 4) due to the samples being able to more accurately approximate the true Kalman filtering distribution. The BNN has lower RMSEs than the NN in all experiments and achieves results close to the best-case scenario for u and h for a large ensemble size of 400. However, the NN is more beneficial to the RMSE/spread ratio than the BNN which is likely due to the small parameter spread of the BNN. The parameter estimates of the NN do not exhibit any sensitivity to the state ensemble size. The sensitivity of the BNN can be explained due to the ensemble size directly controlling the training size and more training data usually increases the predictive capabilities of ANNs. For $N_{ens} > 100$ however, the RMSEs of the parameters seem to saturate which could be caused by the very small network size of only 2 neurons per hidden layer and might positively be influenced by increasing the neurons of the hidden layers. To test this hypothesis, network size sensitivity experiments are conducted in Figure 5. For the results shown in Figure 5 the same 100 experiments as before are conducted with the state ensemble size set to 200 and varied neurons per hidden layer. Contrary to our hypothesis, the parameter RMSEs increase with an increase in neurons as does the spread. This surprisingly has a positive effect on the rain r where the RMSE decreases while its spread increases. The velocity u and fluid height h on the other hand show no sensitivity to the network size. Figure 5 indicates that not only the accuracy of the parameter estimation but also its spread is relevant for the state error. The NN and BNN_0 are trained on the full grid, but observations in real-life settings are usually sparse. Therefore, their sensitivity to the *observation size* was investigated, which is here defined as the percentage of observed grid points. Instead of observing only those grid points whose rain values exceed a certain threshold, as in the previous experiments, percentages corresponding to the values of the x-axis in Figure 6 of random grid points were observed. The RMSEs of the atmospheric variables, especially those of u and h , show a strong sensitivity on the observation size and decrease with more observations available. The parameter RMSEs of the NN, on the other hand, show almost no sensitivity at all.

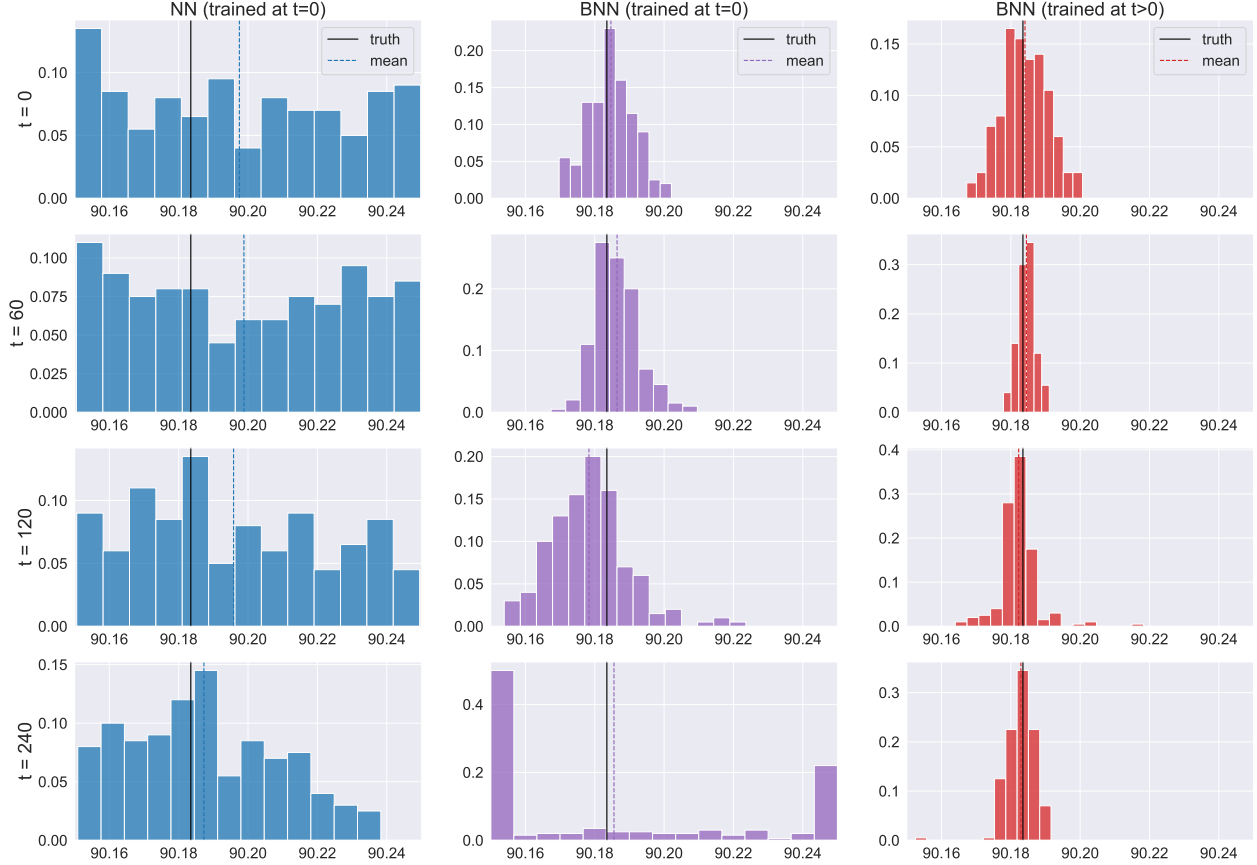


Figure 3: Probability histograms of estimates for rain threshold h_r of one single experiment for NN (left), BNN_0 (middle), and BNN_0+BNN_t (right) over time with 200 ensemble members

The BNN exhibits a slightly stronger sensitivity compared to the NN up until around 60% of available observations. This low sensitivity on the observation size indicates that although the ANNs are trained on the whole grid, only a small number of grid points could actually be relevant for the ANNs' prediction. To investigate this hypothesis the LRP algorithm described in Section 4.1 is utilized in Figures 7 to 10 with the NN since to the best of our knowledge, LRP has not been applied to BNNs so far. For Figure 7 LRP was applied to all three parameters α , ϕ_c and h_r for 100 inputs and averaged. The inputs used in these experiments are observations taken from the true atmospheric state of fully observed grids. To better compare the NN inputs (observations of the state) with their corresponding LRP heatmaps, the values of u, h, r and the LRP heatmap values were rescaled between 0 and 1 and plotted together as heatmaps. The x-axis represents the 250 grid points while the y-axis has no meaning and just provides a spatial dimension so that the colors of the heatmap are visualized better. Darker red tones correspond to higher values and thus represent grid points that were more relevant for the NN's prediction. The total relevances plotted in Figure 7 are simply the LRP heatmap values of one parameter for a certain atmospheric variable summed and divided by the total sum of LRP heatmap values for that parameter. Even though all experiments conducted so far indicate that r is the most sensitive variable to the parameter estimation, for the NN h is the most relevant variable while u and r exhibit roughly the same relevance. It is also surprising that even though the results plotted in Figure 7 are averaged over many experiments, one can still determine distinct lines over certain grid points. These distinct lines indicate that the NN uses only a small number of grid points to make its prediction instead of the whole grid. Using only a small number of important grid points as the input would in turn decrease the number of learnable parameters and might result in the need for much smaller training sizes. This finding would also explain why the sensitivity on the observation size is so low. The heatmaps of u and r look very similar to the input indicating that those grid points with strong winds and rain are especially relevant for the NN. The heatmaps of h however look very different from their input. In Figure 8 the heatmaps of a single experiment are plotted for all three parameters to investigate which grid points are relevant and if the heatmaps of the three parameters indeed look as similar as Figure 7 indicates. Instead of plotting the LRP heatmaps and the atmospheric variable values as heatmaps, in Figure 8 they are visualized as graphs with the x-axis corresponding to the

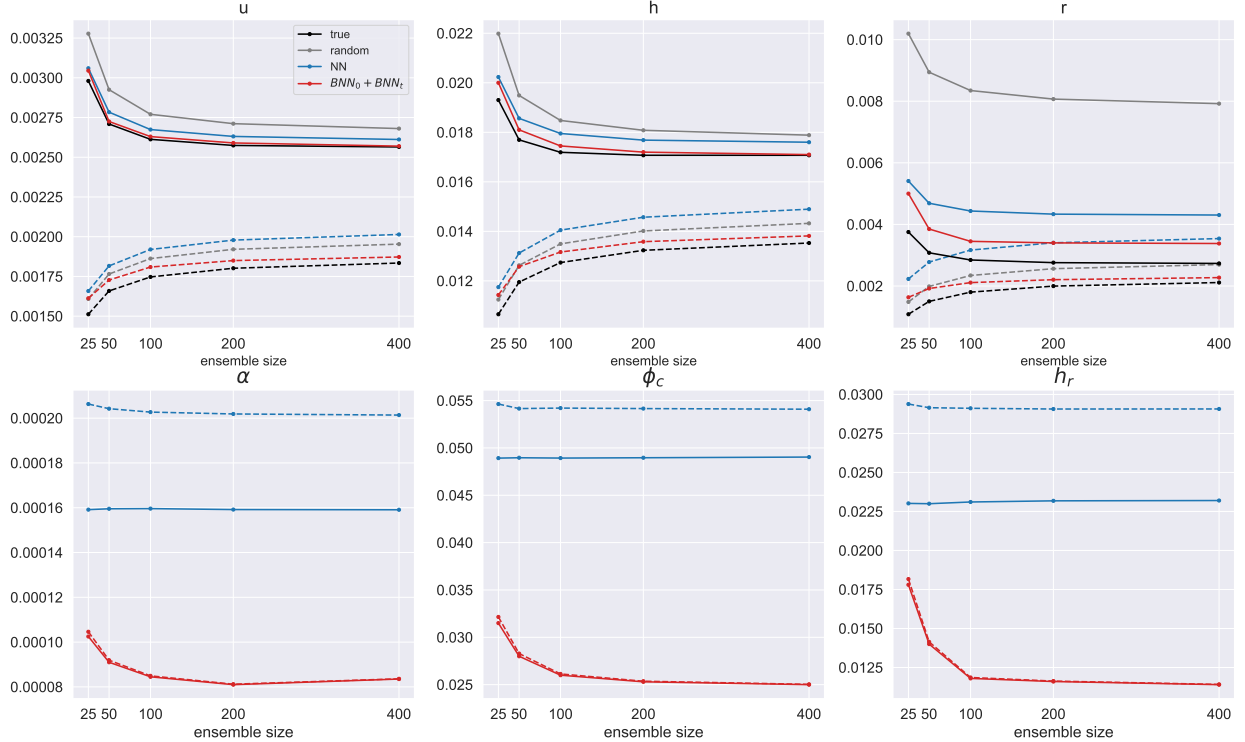


Figure 4: RMSE (solid) and ensemble spread (dashed) of atmospheric variable estimates (upper panel) and parameter estimates (lower panel) against analysis ensemble size averaged over last 100 DA cycles of 100 experiments

grid points and the y-axis corresponding to the rescaled values. The shaded areas represent the values of u, h, r while the red stars are the heatmap values for α of the corresponding inputs. Visualizing the LRP outputs this way makes it even more obvious that grid points with strong winds and rain are very relevant for the NN, although there does not seem to be a distinct relationship between h and its corresponding LRP heatmap. If one plots the LRP heatmap α of h together with the rain (not shown), it seems like the relevant grid points of h are the ones where it is in fact raining. This would explain why simply interpolating the observations and using these to estimate the parameters, as was done for in Figure 2, works so well. From a physical standpoint, it is rather surprising that the heatmaps in Figure 7 look so similar for all three parameters. To check if this is simply due to the fact that they are predicted simultaneously, the same experiments as in Figure 7 are repeated with three individually trained NNs, one for each parameter. For the results in Figure 9 three training and test data-sets are generated: each time keeping two of the parameters constant while varying the parameter that is wished to be estimated. In this setup, there is a clear distinction between the heatmaps of the three individual parameters and also between the heatmaps of Figure 7 and Figure 9. The relevances shift from the fluid velocity u and height h towards the rain r for all three parameters, especially for ϕ_c and h_r where the rain is now the most relevant variable. For the rain removal rate α the most relevant variable is still h . While in Figure 7 the relevances are concentrated on a few single grid points they are more spread out over the grid in Figure 9. To investigate if this spread is due to the averaging over many experiments the same plot as in Figure 8 is created for the three individually trained NNs for the same experiment. When comparing Figure 8 with Figure 10 it becomes apparent that when the NNs are trained for each parameter individually, almost all rainy grid points are now relevant for the NN's prediction instead of just a select few.

5 Conclusion

In this study two types of ANNs are trained to estimate the tunable model parameters of the convective-scale modified shallow water model [Würsch and Craig, 2014]. In the perfect model experiments the NN as well as the BNN are able to decrease the state errors of the atmospheric variables compared to the case where no parameter estimation is applied. The largest reduction of the state error is ultimately found in the rain r . Furthermore, the ANNs investigated here provide tools to quantify the uncertainty of the parameter estimation which increases the ensemble spread of

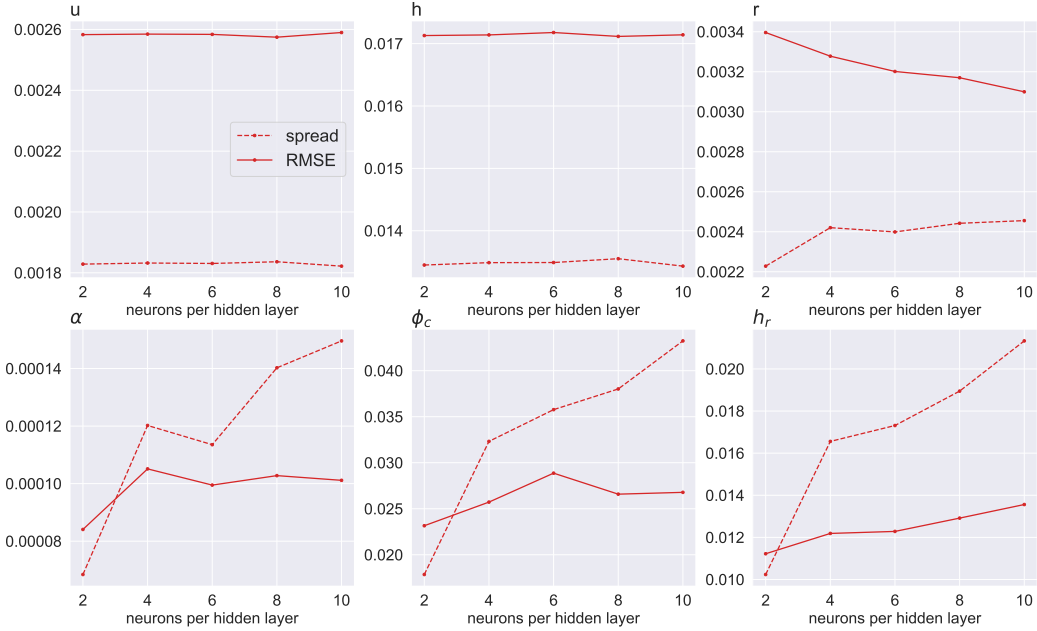


Figure 5: RMSE (solid) and ensemble spread (dashed) of atmospheric variable estimates (upper panel) and parameter estimates (lower panel) against network size in neurons per hidden layer averaged over last 100 DA cycles of 100 experiments using BNN_0+BNN_t with 200 state ensemble members

the state analysis and forecast while decreasing their RMSEs. Interestingly, even though the rain exhibits the largest sensitivity on the parameter estimation, the LRP algorithm shows that the fluid height h was the most relevant variable for the NN’s prediction. In summary, the BNN produced more accurate estimates while needing less training time and hyperparameter tuning.

All experiments conducted in this study assume parameters that are constant in time and space. Future work testing the ANNs’ ability to estimate local and temporal parameters is therefore required. Furthermore, the training data utilized in this study are snapshots of the grid at one point in time. Alternatively, one could investigate the use of different features such as time series of one or more grid points. By utilizing not only atmospheric variables as input features but also ‘climatological predictors’, such as latitude, longitude, time of the day and month, [Bonavita and Laloyaux, 2020] show that the predictive abilities of the ANNs are greatly enhanced. Providing the ANN with information on the geographical location, diurnal cycle, and seasonal cycle during the training is an interesting approach that could have potential benefits for the parameter estimation problem as well. It should be noted that the training data, as well as the observations, are generated by the same simplistic model and it is not clear how well the ANNs’ predictive ability translates to more complex models and real observations. Before testing them in more realistic scenarios, it is necessary to scale down their demand for large training sizes, possibly by reducing the number of input features or number of hidden layers as demonstrated here. Indeed, the LRP heatmaps show that if all parameters are estimated simultaneously the NN makes use of only a few select grid points.

Another possibility to address the here mentioned challenges would be to investigate an alternative kind of stochastic ANN. Leinonen et al. [2020] successfully train a stochastic generative adversarial network (GAN) to downscale time-evolving images of atmospheric fields from low to high resolution. The GAN trained in Leinonen et al. [2020] consists of convolutional and recurrent layers and is able to predict images larger than those it was trained on and can predict longer time series than the sequences used for training. This reduces the need for large training sizes and offers the possibility for offline training.

In the studied test case, with perfect model assumptions and enough training data, the ANNs were able to estimate the unknown model parameters and quantify their uncertainty more accurately than a simple linear regression, even under sparse and noisy conditions. Including the parameter estimates obtained from the ANNs in the DA cycle resulted in

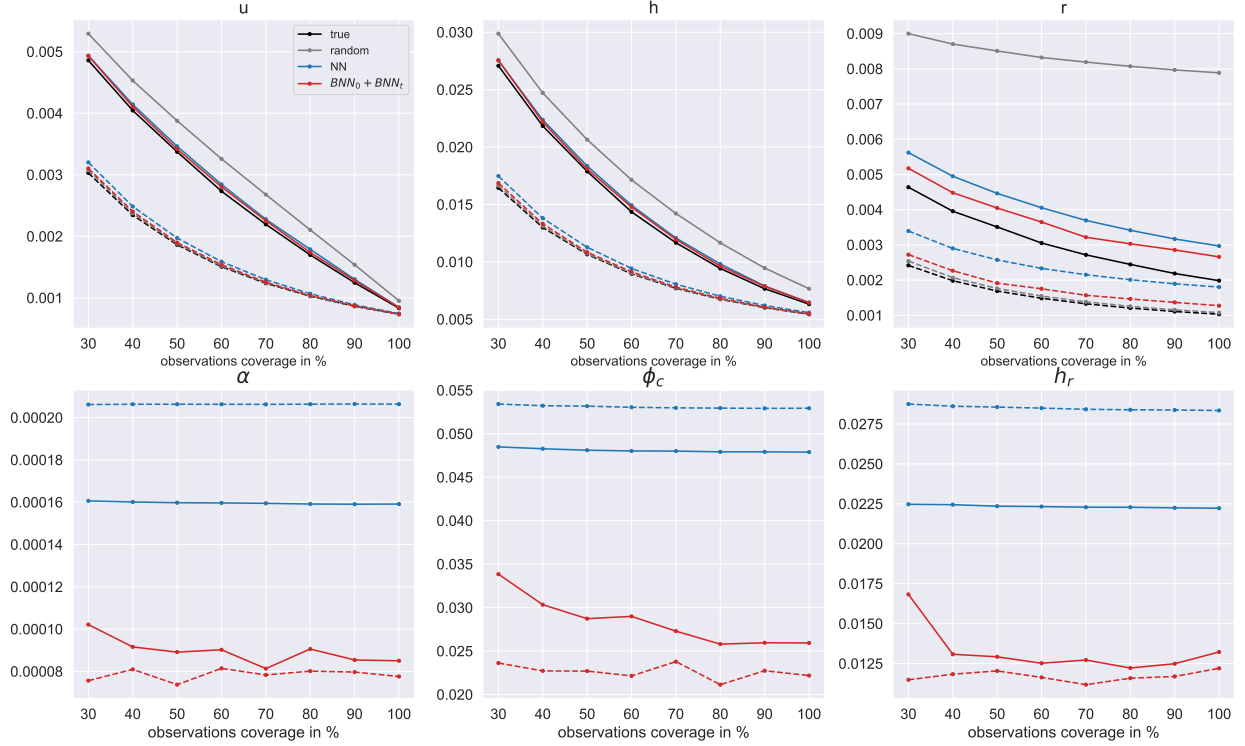


Figure 6: RMSE (solid) and ensemble spread (dashed) of atmospheric variable estimates (upper panel) and parameter estimates (lower panel) against observation coverage with 50 ensemble members averaged over last 100 DA cycles averaged over 100 experiments

reduced state errors and increased ensemble spreads compared to the case without parameter estimation and unknown parameters.

6 Acknowledgements

The research leading to these results has been done within the subproject B6 of the Transregional Collaborative Research Center SFB / TRR 165 “Waves to Weather” funded by the German Research Foundation (DFG). T. Janjić is also grateful to the DFG for funding of her Heisenberg Award (DFG JA1077/4-1).

Conflict of interest

The authors declare that they have no conflict of interest.

References

- P.A. O’Gorman and J.G. Dwyer. Using machine learning to parameterize moist convection: Potential for modeling of climate, climate change, and extreme events. *Journal of Advances in Modeling Earth Systems*, 10(10):2548–2563, 2018.
- S. Rasp, M.S. Pritchard, and P. Gentine. Deep learning to represent sub-grid processes in climate models, 2018.
- J. Yuval and P.A. O’Gorman. Stable machine-learning parameterization of subgrid processes for climate modeling at a range of resolutions. *Nature Communications*, 11(1), 2020.
- R.S. Cintra and H.F. de Campos Velho. Data assimilation by artificial neural networks for an atmospheric general circulation model: Conventional observation. *CoRR*, abs/1407.4360, 2014.

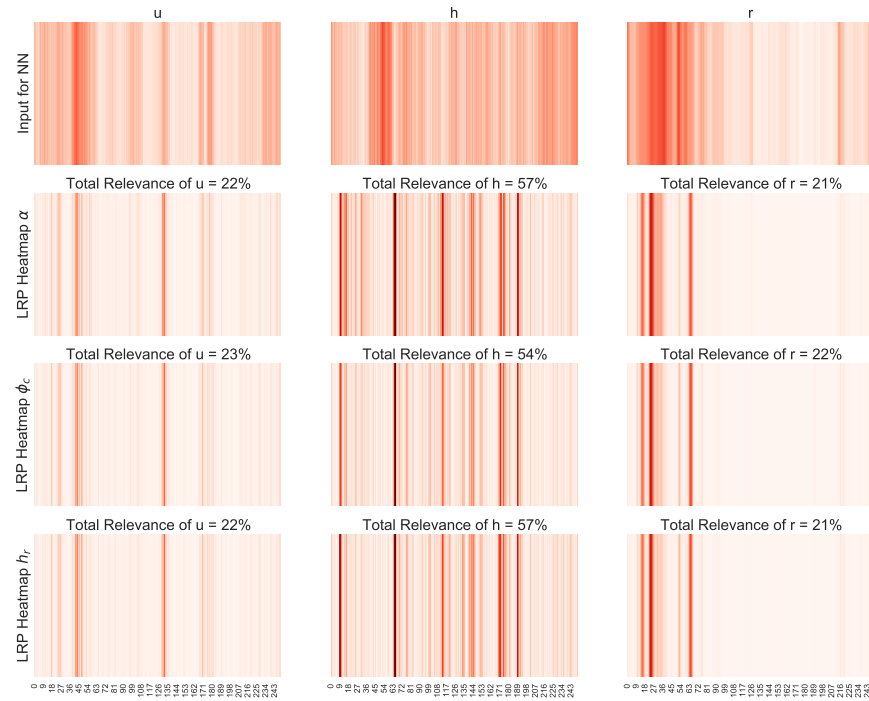


Figure 7: Input (first row) and corresponding LRP heatmaps for α (second row), ϕ_c (third row) and h_r (last row) against grid points of NN trained according to Section 3.2 averaged over 100 experiments

- J. Brajard, A. Carrassi, M. Bocquet, and L. Bertino. Combining data assimilation and machine learning to emulate a dynamical model from sparse and noisy observations: A case study with the Lorenz 96 model. *Journal of Computational Science*, 44:101171, 2020.
- A. Farchi, P. Laloyaux, M. Bonavita, and M. Bocquet. Using machine learning to correct model error in data assimilation and forecast applications. 2021. doi:10.1002/qj.4116.
- M. Bonavita and P. Laloyaux. Machine learning for model error inference and correction. *Journal of Advances in Modeling Earth Systems*, 12, 2020.
- Y. Ruckstuhl, T. Janjić, and S. Rasp. Training a convolutional neural network to conserve mass in data assimilation. *Nonlinear Processes in Geophysics*, 28(1):111–119, 2021.
- T. Janjić, D. McLaughlin, S.E. Cohn, and M. Verlaan. Conservation of mass and preservation of positivity with ensemble-type Kalman filter algorithms. *Monthly Weather Review*, 142:755–773, 2014.
- M. Trautner, G. Margolis, and S. Ravela. Informative neural ensemble Kalman learning. *CoRR*, abs/2008.09915, 2020.
- N. Yadav, S. Ravela, and A.R. Ganguly. Machine learning for robust identification of complex nonlinear dynamical systems: Applications to earth systems modeling, 2020.
- E.N. Lorenz. Designing chaotic models. *Journal of the Atmospheric Sciences*, 62:1574–1587, 2005.
- C.E. Rasmussen and C.K.I. Williams. *Gaussian Processes for Machine Learning*. MIT Press, 2006.
- Y. M. Ruckstuhl and T. Janjić. Parameter and state estimation with ensemble Kalman filter based algorithms for convective-scale applications. *Quarterly Journal of the Royal Meteorological Society*, 144(712):826–841, 2018. doi:https://doi.org/10.1002/qj.3257.
- Y. Ruckstuhl and T. Janjić. Combined state-parameter estimation with the letkf for convective-scale weather forecasting. *Mon. Wea. Rev.*, 148(4):1607–1628, 2020. doi:10.1175/MWR-D-19-0233.1. URL <https://doi.org/10.1175/MWR-D-19-0233.1>.
- B.A. Toms, E.A. Barnes, and I. Ebert-Uphoff. Physically interpretable neural networks for the geosciences: Applications to earth system variability. *Journal of Advances in Modeling Earth Systems*, 12(9), 2020.
- Z.M. Labe and E.A. Barnes. Detecting climate signals using explainable AI with single-forcing large ensembles. *Earth and Space Science Open Archive*, page 40, 2021.

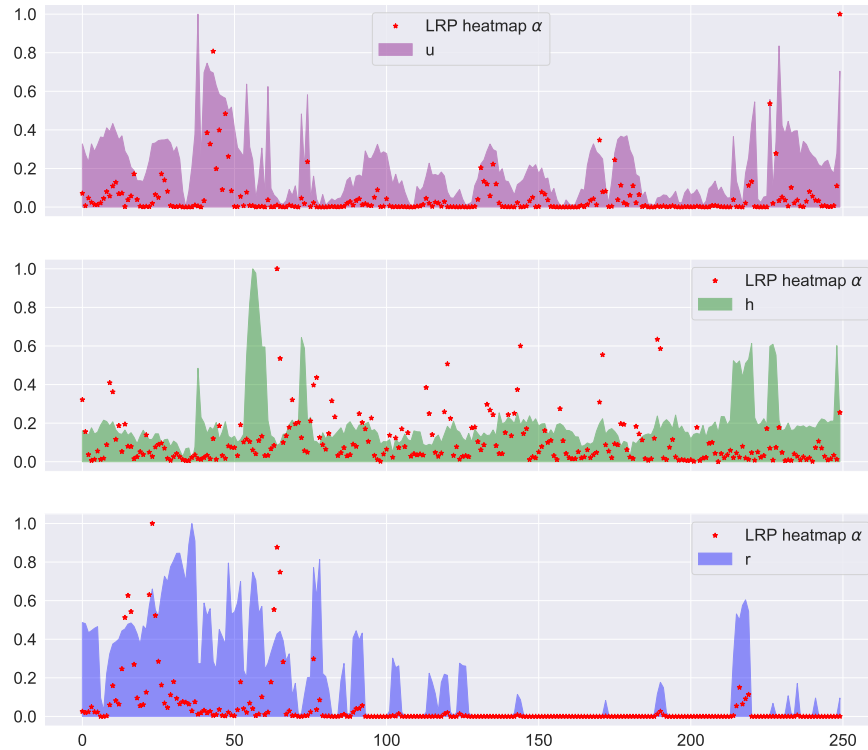


Figure 8: Rescaled values of fluid velocity u (upper panel), height h (middle panel), rain r (lower panel), and corresponding LRP heatmaps α (red stars) of NN trained according to Section 3.2 against all 250 grid points for a single experiment

- M. Würsch and G.C. Craig. A simple dynamical model of cumulus convection for data assimilation research. *Meteorologische Zeitschrift*, 23(5):483–490, 2014.
- G. Evensen. Sequential data assimilation with a nonlinear quasi-geostrophic model using monte carlo methodsto forecast error statistics. *J. Geophys. Res.*, 99:10,143–10,162, 1994.
- G. Evensen. The ensemble kalman filter: theoretical formulation and practical implementation. *Ocean Dynamics*, 53: 343–367, 2003.
- B. Lakshminarayanan, A. Pritzel, and C. Blundell. Simple and scalable predictive uncertainty estimation using deep ensembles, 2017.
- L.V Jospin, W. Buntine, F. Boussaid, H. Laga, and M. Bennamoun. Hands-on bayesian neural networks – a tutorial for deep learning users, 2020.
- D.J.C. MacKay. A practical bayesian framework for backpropagation networks. *Neural Comput.*, 4:448–472, 1992.
- S. Ioffe and C. Szegedy. Batch normalization: Accelerating deep network training by reducing internal covariate shift. *CoRR*, abs/1502.03167, 2015.
- A. Labach, H. Salehinejad, and S. Valaee. Survey of dropout methods for deep neural networks. *CoRR*, abs/1904.13310, 2019.
- Lu Lu. Dying relu and initialization: Theory and numerical examples. *Communications in Computational Physics*, 28 (5):1671–1706, Jun 2020.
- M.D. Hoffman, D.M. Blei, C. Wang, and J. Paisley. Stochastic variational inference. *J. Mach. Learn. Res.*, 14: 1303–1347, 2013.
- D.P. Kingma and J. Ba. Adam: A method for stochastic optimization. *CoRR*, abs/1412.6980, 2014.
- A. Paszke, S. Gross, F. Massa, A. Lerer, J. Bradbury, G. Chanan, T. Killeen, Z. Lin, N. Gimelshein, L. Antiga, A. Desmaison, A. Köpf, E. Yang, Z. DeVito, M. Raison, A. Tejani, S. Chilamkurthy, B. Steiner, L. Fang, J. Bai, and S. Chintala. Pytorch: An imperative style, high-performance deep learning library. *CoRR*, abs/1912.01703, 2019.

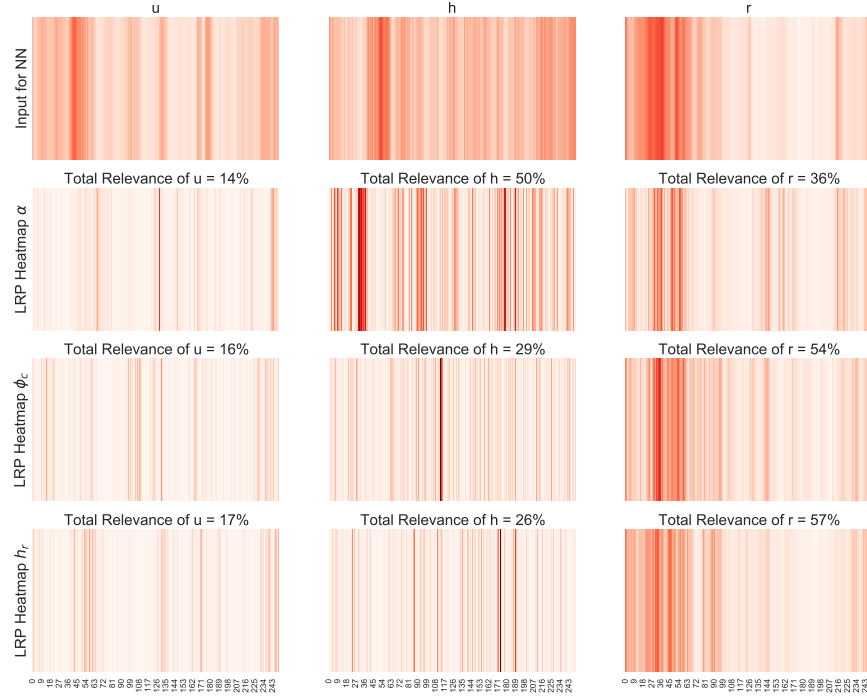


Figure 9: Input (first row) and corresponding LRP heatmaps for α (second row), ϕ_c (third row) and h_r (last row) against grid points of 3 individually trained NNs averaged over 100 experiments

- E. Bingham, J.P. Chen, M. Jankowiak, F. Obermeyer, N. Pradhan, T. Karaletsos, R. Singh, P.A. Szerlip, P. Horsfall, and N.D. Goodman. Pyro: Deep universal probabilistic programming. *CoRR*, abs/1810.09538, 2018.
- S. Bach, A. Binder, G. Montavon, F. Klauschen, K.R. Müller, and W. Samek. On pixel-wise explanations for non-linear classifier decisions by layer-wise relevance propagation. *PLoS ONE*, 10(7), 2015.
- M. Böhle, F. Eitel, M. Weygandt, and K. Ritter. Layer-wise relevance propagation for explaining deep neural network decisions in mri-based alzheimer’s disease classification. *Frontiers in Aging Neuroscience*, 11, 2019.
- J. Leinonen, D. Nerini, and A. Berne. Stochastic super-resolution for downscaling time-evolving atmospheric fields with a generative adversarial network. *IEEE Transactions on Geoscience and Remote Sensing*, page 1–13, 2020.

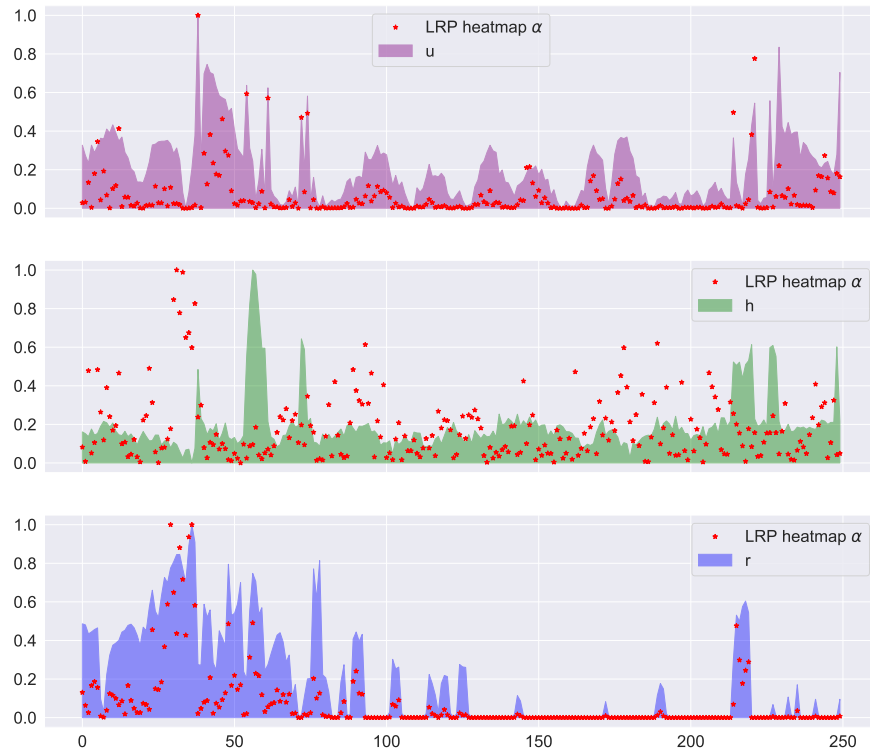


Figure 10: Rescaled values of fluid velocity u (upper panel), height h (middle panel), rain r (lower panel), and corresponding LRP heatmaps α (red stars) of 3 individually trained NNs against all 250 grid points for a single experiment